

## **Effect of WENO advection scheme on simulation of stratocumulus-topped atmospheric boundary layer**

Hannah L. Hagen

### **ABSTRACT**

Clouds maintain Earth's energy balance and are a key regulator of weather and climate. The effect of the WENO advection scheme was analyzed in simulation of the marine stratocumulus-topped boundary layer. Data from the first research flight (RF01) of the DYCOMS II field campaign was used as a test case. RF01 was characterized by a cloud layer that was maintained throughout the night with a strong, sharp inversion at cloud top. Cloud Model 1 (CM1) was used to simulate a 3.36 km x 3.36 km x 2.0 km domain. Two coarse simulations (15 m), one using the WENO advection scheme and the other using the default advection scheme for CM1 were compared with a high resolution (5 m) simulation that closely matched the observations from RF01. Global integrals like domain liquid water and vertical velocity statistics reveal that the WENO scheme produced results that were highly divergent from the high resolution simulation. In contrast, the default advection scheme of CM1, which is a 5<sup>th</sup> order scheme with mass flux correction, was a closer match to the high resolution data. The results and analysis indicate that the WENO scheme produced artificially large entrainment of warm and dry air into the cloud layer, weakening radiative cooling and reducing turbulent mixing beneath the cloud layer. The result of this artificial entrainment in the WENO simulation was a decoupled boundary layer and nearly complete dissipation of the cloud layer by the end of the four-hour simulation period. On the other hand, the simulation using the default advection scheme produced a thinner, but still present, cloud layer, suggesting significantly less artificial entrainment of dry air into the cloud layer. The divergent results indicate that simulation of marine stratocumulus is highly sensitive to numerical diffusion at cloud top. This increased numerical diffusion at cloud top produced by the WENO scheme led to incorrect decoupling and dissipation of the cloud layer. On the other hand, the default advection scheme showed closer agreement with the high resolution simulation and observations, although this improved performance was achieved at a greater computational cost. An ideal advection scheme would reduce both numerical diffusion and oscillations at sharp gradient, but also maintain the computational efficiencies of a scheme like WENO.

### **KEYWORDS**

Cloud-resolving model, numerical analysis, WENO schemes, marine stratocumulus, large eddy simulation (LES)

## 1. Introduction

Clouds maintain energy balance and are a key regulator of weather and climate. It is estimated that even small changes in the scope or location of clouds may change the climate more than or as much as the anticipated changes caused by greenhouse gases, human-produced aerosols, or other factors. Yet, our understanding of and ability to accurately model clouds is greatly limited. Computer simulation of the atmosphere is critical to understanding and predicting short-term weather and long-term global climate. According to the International Panel on Climate Change (IPCC) Fifth Assessment Report, clouds and aerosols continue to contribute the largest uncertainty to estimates and interpretations of the Earth's changing energy budget and climate (IPCC 2013).

Most atmospheric simulations are based on the Navier-Stokes equations of fluid motion discretized on a finite grid (see Appendix A for detailed description). To reduce the computational expense, most fine-scale models use a large eddy simulation (LES) that resolves large eddies responsible for the bulk of momentum, energy and mass transport and models subgrid contributions often using an eddy viscosity model. Because it is impossible to represent the planetary boundary layer (PBL) with fidelity in the laboratory and observing the PBL is difficult and expensive, LES studies are often the basis for developing and testing theories.

Previous studies have questioned the ability of large eddy simulations (LESs) to represent the turbulent structure of stratocumulus-topped boundary layers (Moeng et al., 1996, Stevens et al., 2001, Stevens 2002, Stevens et al., 2005). Stratocumulus is the most common cloud type globally, covering approximately 20% of Earth's surface at any given time (Warren et al. 1986, 1988) and therefore critical to climate. Turbulence in marine stratocumulus-topped boundary layers is driven by radiative cooling at cloud top: air at cloud top cools due to longwave radiation and sinks toward the surface, driving turbulence in the boundary layer. See Fig. 1 for a sketch of the mean thermodynamic profile of marine stratocumulus observed by the DYCOMS-II field campaign (Stevens et al., 2007). This is an "upside-down" version of turbulence in most boundary layers over land, which are dominated by convective eddies driven by surface heating.

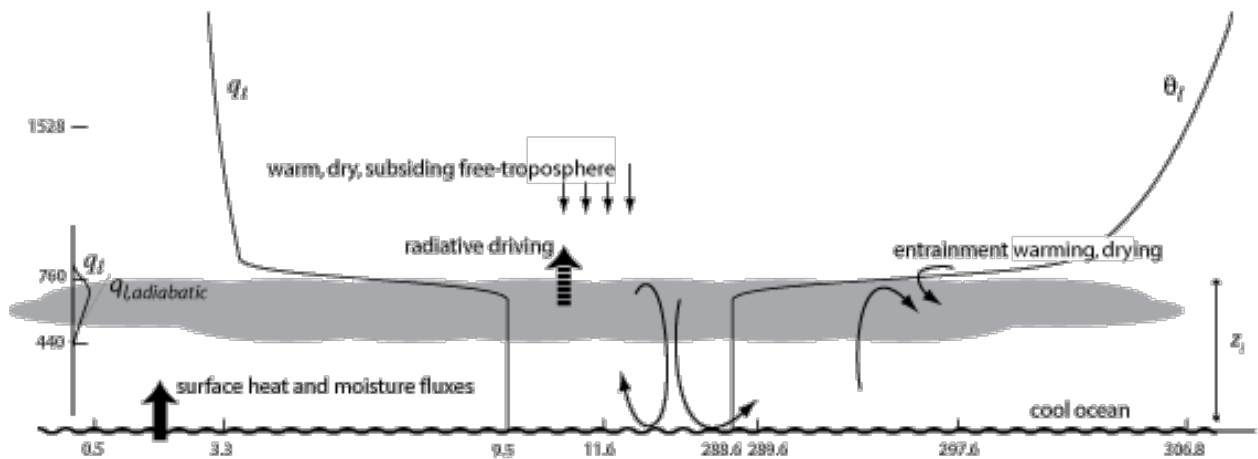


FIG. 1 Schematic of mean stratocumulus structure observed during the Marine Stratocumulus (DYCOMS-II) field campaign. The potential temperature, specific humidity and height at 850 hPa are indicated, as are values within and just above the STBL. Source: Stevens et al., 2007.

Moeng et al., 1996 compared 12 different large eddy simulations (LESs) of stratocumulus-topped PBL and found that global integrals, like liquid water path, varied by as much as an order of magnitude between simulations. Moeng et al., 1996 attributed this difference to the extent to which different models entrained warm and dry air from above the inversion into the turbulent planetary boundary layer. Lilly 1968 and Bretherton et al., 1999 attempted to isolate the effect on entrainment on stratocumulus-topped PBL through an idealized “smoke cloud” simulation. They concluded that fine vertical resolution (on the order of 5 m) was required to produce entrainment rates with little scatter amongst models; lower vertical resolution led to sizable differences in entrainment rates between models. Stevens et al., 2005 tested the fidelity of 16 large eddy simulations (LESs) in representing the turbulent structure of stratocumulus-topped boundary layer observed on the first research flight of the Marine Stratocumulus (DYCOMS-II) field campaign. Stevens et al., 2005 found that most models in their native configuration greatly overestimated mixing at cloud top, tending toward a decoupled layer in which liquid water path and turbulent intensities were grossly underestimated. Stevens et al., 2005 also concluded that global behavior of the solution depended heavily on the numerics and the SG models in regions of sharp gradients and phase changes (e.g. the inversion at cloud top).

I evaluate the effect of two different advection schemes on simulation of stratocumulus-topped boundary layer observed on the first research flight of the Marine Stratocumulus (DYCOMS-II) field campaign. I test a 5<sup>th</sup> order advection scheme with mass flux correction and the WENO, weighted essentially non-oscillatory, advection scheme at 15 m vertical resolution

and compare the resultant turbulent structures with results from a simulation at high resolution (5 m) and observational data. I chose to analyze the impact of advection schemes because, aside from the SG model, advection plays an important role in determining the entrainment rate at cloud top. Furthermore, WENO advection scheme was chosen for this study because it is advocated to improve solutions near high gradient and previous studies (Moeng et al., 1996, Stevens et al., 2001, Stevens 2002, Stevens et al., 2005) reveal that the global solution is highly dependent on the solution at the sharp inversion layer.

## 2. WENO Advection Scheme

The WENO scheme is a finite difference method that numerically approximates solutions of hyperbolic partial differential equations (PDEs) and other convection dominated problems with high order accuracy in smooth regions and essentially non-oscillatory transition at solution discontinuities or high gradients (Shu 2003 and Shu 1989/1999 lecture notes). WENO uses adaptive stencils in the reconstruction procedure, achieving 5<sup>th</sup> order accuracy on smooth regions in the solution and dropping to 3<sup>rd</sup> order accuracy at regions with discontinuities by omitting the stencil that produces artificial oscillation. The main advantage of this scheme is its capability to achieve high order formal accuracy in smooth regions while maintaining stable, non-oscillatory and sharp discontinuity transitions (Shu 2011). According to Shu 2011, the schemes are especially suitable for problems containing both strong discontinuities and complex smooth solution features. Marine stratocumulus contains a smooth solution throughout the boundary layer with a high gradient in temperature and moisture at cloud top.

I use the 5<sup>th</sup> order accurate WENO scheme designed by Jiang and C.-W. Shu 1996. The WENO scheme at its core is an approximation procedure. The following simple example of interpolation, provided by Shu 2011, is used here to describe this approximation procedure. Assume that we are given a uniform mesh  $\dots < x_1 < x_2 < x_3 < \dots$  and the point values of a function  $u_i = u(x_i)$ . We would like to find an approximation of the function  $u(x)$  at a point other than the nodes  $x_i$ , for example at the half nodes  $x_{i+1/2}$ .

Following the traditional approach to interpolation, we could find a unique polynomial of degree at most two, denoted by  $p_1(x_{i+1/2})$ , which interpolates the function  $u(x)$  at the mesh

points in the stencil  $S_1 = \{x_{i-2}, x_{i-1}, x_i\}$ . We could then use  $u_{i+1/2}^{(1)} \equiv p_1(x_{i+1/2})$  as an approximation to the value  $u(x_{i+1/2})$ , which is given explicitly as

$$u_{i+1/2}^{(1)} = \frac{3}{8}u_{i-2} - \frac{5}{4}u_{i-1} - \frac{15}{8}u_i$$

and is third order accurate if the function  $u(x)$  is smooth in the stencil  $S_1$ . Similarly, we could choose two other stencils  $S_2 = \{x_{i-1}, x_i, x_{i+1}\}$  and  $S_3 = \{x_i, x_{i+1}, x_{i+2}\}$  to obtain interpolation polynomial approximations  $u_{i+1/2}^{(2)}$  and  $u_{i+1/2}^{(3)}$  that are also third order accurate. For example:

$$u_{i+1/2}^{(2)} = -\frac{1}{8}u_{i-1} + \frac{3}{4}u_i + \frac{3}{8}u_{i+1}$$

$$u_{i+1/2}^{(3)} = \frac{3}{8}u_i + \frac{3}{4}u_{i+1} - \frac{1}{8}u_{i+2}$$

Each of these approximations alone is third order accurate, but using a large stencil  $S = \{x_{i-2}, x_{i-1}, x_i, x_{i+1}, x_{i+2}\}$ , which is the union of all three third order stencils  $S_1, S_2, S_3$ , then we would be able to obtain an approximation that is 5<sup>th</sup> order accurate. The WENO procedure obtains a 5<sup>th</sup> order accurate approximation by using a convex combination of the three third-order approximations:

$$i_{i+1/2} = w_1 u_{j+1/2}^{(1)} + w_2 u_{i+1/2}^{(2)} + w_3 u_{i+1/2}^{(3)}$$

where  $w_j \geq 0$  and  $w_1 + w_2 + w_3 = 1$ . The nonlinear weights  $w_j$  satisfy the following requirements:

- $w_j \approx \gamma_j$  if  $f(u)$  is smooth in the big stencil  $S$ . Where  $\gamma_j$  are linear weights.
- $w_j \approx 0$  if  $f(u)$  has a discontinuity in the stencil  $S_j$  but it is smooth in at least one of the other two stencils.

The choice of the nonlinear weights  $w_j$  relies on the smoothness indicator  $\beta_j$ , which measures the relative smoothness of the function  $u(x)$  in the stencil  $S_j$ .

In summary, WENO uses a convex combination of all the candidate stencils, each assigned a non-linear weight which depends on the local smoothness of the numerical solution based on that stencil. This method achieves 5<sup>th</sup> order accuracy on regions of smooth regions in the solution and 3<sup>rd</sup> – 5<sup>th</sup> order accuracy on regions with high gradients or discontinuities.

### 3. Test case and simulation set up

#### a. Test case: DYCOMS-II, RF01

The first research flight (RF01) of the Dynamics and Chemistry of Marine Stratocumulus (DYCOMS-II) field study (detailed in Stevens et al., 2003a and Stevens et al., 2003b) served as our test case. A main motivation for this campaign was to test differences between LES models. Previous studies have found that different LES models led to markedly different entrainment parameterizations with overall entrainment rates differing by a factor of 2 or more, even for fine vertical resolution (Stevens 2002). This study is an extension of studies like Stevens et al., 2005, because it looks like how a modification to LES codes, namely choice of advection scheme, impacts entrainment and the overall simulation result. Furthermore, this test case rests in an interesting region of parameter space, on the boundary where cloud top mixing is predicted to render the cloud layer unstable by some theories, or lead to decoupling and dissipation by other theories (e.g. Randall 1980, Deardorff 1980a). Yet, the results show a stable cloud layer that is maintained throughout the night. Thus, this test case is a promising and unique opportunity to test the effect of advection scheme on entrainment parameterizations in a case study that is particularly sensitive to cloud top mixing and decoupling.

The conditions of this case were well-suited for many reasons: the environmental conditions, such as temperature, moisture, velocity, heat/moisture flux were largely homogeneous; there was no drizzle, which is difficult to model; and other groups have successfully simulated the case. Our simulation occurs at night because the forcings (radiation, surface sensible and latent heat flux) are easier to characterize and more stationary.

I use the following mean conditions, replicated from an LES inter-comparison study based on the same test case (Stevens et al., 2005), to initialize and force our simulation.

## 1) Mean State

The basic state was replicated from Stevens et al., 2005, who calculated the basic state from all the measurements of RF01 and idealized a quasi-two-layer structure in liquid water potential temperature and total-water specific humidity (Fig. 2) according to:

$$\theta_1 = \begin{cases} 289.0 \text{ K}, & z \leq z_i \\ 297.5 + (z - z_i)^{1/3} \text{ K}, & z > z_i \end{cases}$$

$$q_t = \begin{cases} 9.0 \text{ g kg}^{-1}, & z \leq z_i \\ 1.5 \text{ g kg}^{-1}, & z > z_i \end{cases}$$

$$q_c = \begin{cases} 0 \text{ g kg}^{-1}, & z < c_b \\ \frac{z - c_b}{z_i - c_b} * q_{c, \max} \text{ g kg}^{-1}, & c_b \leq z < z_i \\ 0 \text{ g kg}^{-1}, & z \geq z_i \end{cases}$$

where,

$z_i = 840\text{m}$  is the inversion height (cloud top).

$c_b = 600\text{m}$  is the height of the cloud base.

$q_{c, \max} = 0.45 \text{ g kg}^{-1}$  is the liquid water mixing ratio at cloud top.

Based on the initial conditions of Stevens et al., 2005, I initialized a cloud layer from 600m to the inversion height at 840m, with the maximum liquid water mixing ratio  $q_c = 0.45 \text{ g kg}^{-1}$  at

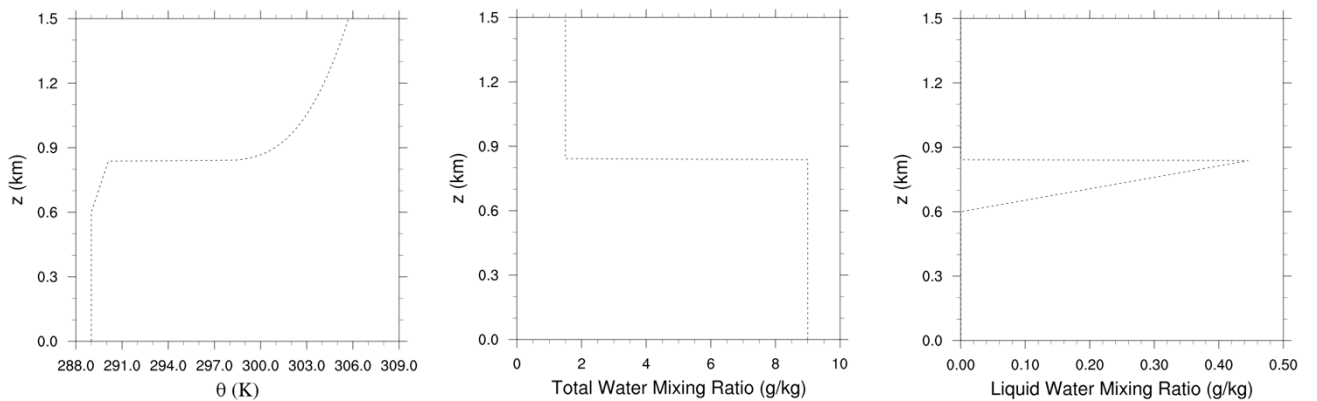


FIG. 2. Initial conditions for potential temperature ( $\theta$ ), total water mixing ratio ( $q_t$ ), and liquid water mixing ratio ( $q_c$ ). We initialized a quasi-two-layer structure in  $\theta$  and  $q_t$ , with a cloud layer from 600m to 840m.

the inversion height, or cloud top (Fig. 2). Stevens et al., 2005 derived  $\theta_l$  from the measured air temperature using physical constants ( $c_p$ ,  $R_d$ ,  $L_v$ ) and a surface pressure of 1017.8 hPa.

Other forcings include geostrophic winds of  $U_g = 7 \text{ m s}^{-1} = 7\text{m/s}$  and  $V_g = -5.5 \text{ m s}^{-1}$  and a constant sea surface temperature of 292.5 K. These initial conditions are based on the observed conditions during RF01.

## 2) Radiative forcing

I used Stevens et al., 2005's parameterization of radiative forcing to closely match the actual radiative forcing of this test case. By prescribing radiation I diminish any error that may originate from the radiation scheme.

### b. Simulation codes and configurations

I use Cloud Model 1 (CM1), developed by the National Center for Atmospheric Research (NCAR), for this study because it is designed as a research tool to better understand cloud dynamics and physics. CM1 is a three-dimensional, non-hydrostatic, non-linear, time-dependent numerical model designed for idealized studies of atmospheric phenomena. The governing equations that underlie CM1 are conservation of mass, momentum, potential temperature, and moisture mixing ratio. I use the compressible form of the Navier Stokes equations for this study. A detailed description of the governing equations and mathematical formulation of CM1 is provided by Bryan 2002.

This study compares three simulations, all of which ran for 4 hours on a horizontal grid of 96 x 96 points with 35m horizontal grid spacing. The first simulation was a high resolution simulation, which serves as our proxy for the "truth" and closely matches observations. In this high resolution simulation, vertical spacing was 5 m below 1 km and stretched using a smooth stretching scheme from 5 m- to 25 m- resolution between 1 km and the top of the domain (2.5 km). The scheme is based on the one presented in Wilhelmson and Chen 1982. This ensured 5 m resolution in the vicinity of the cloud layer. I chose 5 m vertical resolution in the vicinity of the

cloud layer based on the consensus that 5 m vertical resolution is necessary to properly represent entrainment in stratocumulus-like, radiatively driven flows. This consensus emerged from a smoke cloud experiment (Lilly 1968; Bretherton et al., 1999) that showed simulations with vertical resolution poorer than 5 m differed markedly in their resultant entrainment rates, but as vertical resolution was increased, scatter amongst the models declined and they agreed more closely with the laboratory predictions (Bretherton et al., 1999). I chose 35 m horizontal resolution because most studies demonstrate much less sensitivity to horizontal resolution (Lewellen and Lewellen 1998; Stevens et al., 1999). Because horizontal resolution did not markedly change the simulation results in these studies, it can be inferred that PBL-scale eddies determine the rate of entrainment.

I compare the results of the high resolution run to two coarser runs using a 5<sup>th</sup> order advection scheme with mass flux correction and the WENO advection scheme, respectively. Both coarse simulations use 15 m vertical resolution in the vicinity of the cloud layer.

#### 4. Result & Discussion

##### a. High resolution simulation

The high resolution simulation, overall, closely matched the observations from the first research flight of DYCOMS-II field campaign. Profiles of mean variables and velocity statistics are described here and compared to observations. The domain liquid water content, an integral of cloud water over the entire computation domain, decreased sharply by about 20% in the first 30 minutes of the simulation, reaching a minimum at  $t = 1.2$  hr (Fig. 3). Afterwards, the domain liquid water generally increases for the remainder of the simulation, marked by two periods of rapid increase.

There are no direct measurements of cloud water evolution to compare to, however estimates of the temporal evolution of cloud boundaries and liquid water profiles from the aircraft data indicate that the cloud layer maintained its thickness, and perhaps even deepened. Furthermore, cloud fraction, measured during cloud top legs was greater than 99% throughout the night. Despite an initial reduction in the cloud layer, our high resolution simulation is relatively consistent with the observations and maintains the bulk of the cloud layer.

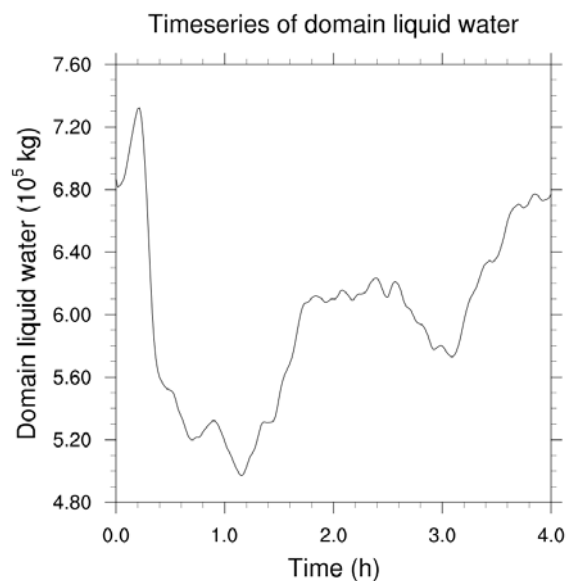


FIG. 3. Time series of domain liquid water (liquid water integrated over the entire computational domain).

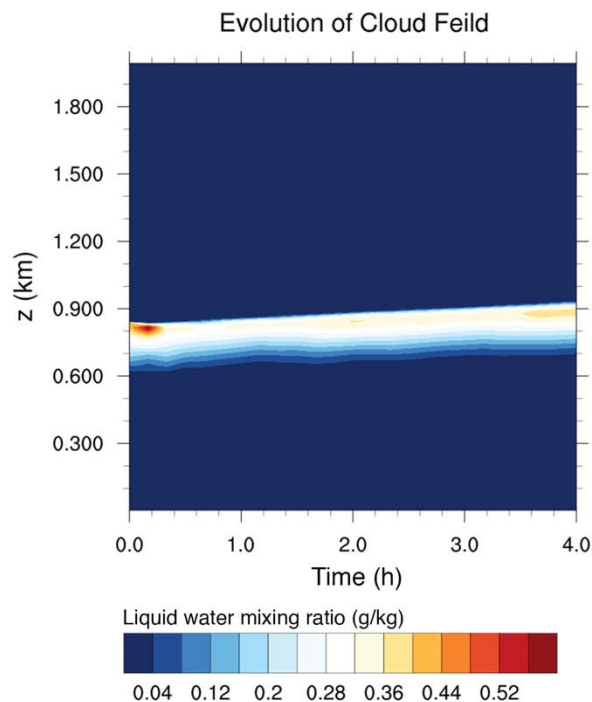


FIG. 4. Time series of the vertical profile of liquid water mixing ratio ( $q_t$ ). The colors represent the liquid water mixing ratio ( $q_t$ ).

It is possible that the drying in the first 1-2 hours is an artefact of the spin-up process. Another possibility is that the model simulates a steady state with less domain liquid water than was observed. By the end of the 4<sup>th</sup> hour, however, the model regains the lost liquid water and domain liquid water content reaches the level prescribed at the start of the simulation.

Cloud top height rises steadily throughout the four-hour simulation, experiencing a total of 90 m lift (Fig. 4). The simulated rise of the inversion height agrees with estimates from aircraft data indicating a rise of the inversion height by 50 m throughout the night. Throughout the simulation, the maximum liquid water mixing ratio is under predicted, averaging approximately 0.32 g/kg, while observations indicate mixing ratios close to 0.45 g/kg at cloud top. At the end of the 4<sup>th</sup> hour, the growing liquid water mixing ratio approaches the observations.

Both the potential temperature profile and the total water mixing ratio profile maintain their pseudo two-layer structure and also exhibit a rise of the inversion by 90 m (Fig. 5). Additionally, the boundary layer evolves to a state approximately 1 degree warmer in potential temperature. The total water profile and potential temperature are constant under cloud top, indicative of a

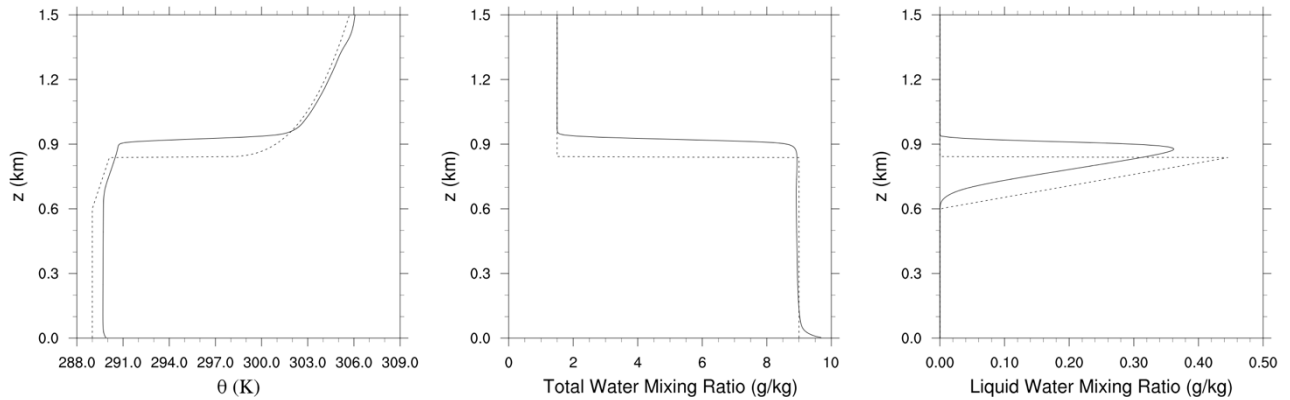


FIG. 5 Vertical profiles of mean potential temperature (left), liquid water mixing ratio (middle) and total water mixing ratio (right) at initial time (dotted line) and averaged over the fourth hour (solid line). Depicts the evolution of the mean structure in moisture and potential temperature.

well-mixed boundary layer. The elevated total water mixing ratio at the surface is expected for marine boundary layers where evaporation is strong.

The variance and skewness of vertical velocity indicate the turbulent structure of the boundary layer. The single peak in variance, occurring at cloud base ( $\sim 700\text{m}$ ), indicates strong turbulence at this height (Fig. 6). The low variance at cloud top suggests a sharp, strong inversion with small fluxes across the capping layer.

Because I only prescribed surface heat fluxes and did not prescribe surface shear, I expect turbulence to grow in strength from the surface, where buoyancy is produced, to cloud base, where turbulent eddies driven by radiative cooling are expected to dominate. The variance data matches our expectation, with variance (a measure of turbulence) increasing from surface until the maximum at cloud base. It also matches in situ and radar measurement shape and magnitude which exhibit a single well-defined peak in  $\overline{w'w'}$  near cloud base of  $\sim 0.5\text{m}^2\text{s}^{-2}$ , close to our  $\sim 0.4\text{m}^2\text{s}^{-2}$ .

The third moment, or the skewness, of vertical velocity provides a measure of the asymmetry of the distribution of vertical velocity perturbations within the boundary layer. The sign of skewness indicates the direction of the flux of turbulent kinetic energy. Positive vertical velocity skewness is indicative of surface-heating-driven convection, in which strong, narrow updrafts are surrounded by larger areas of weaker downdrafts. Cloud top long wave radiative-cooling, on the

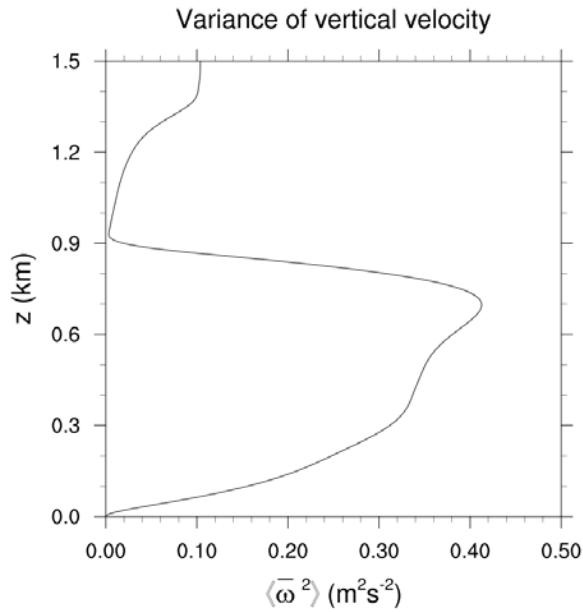


FIG. 6 Vertical profile of variance of vertical velocity averaged over the last two hours of the simulation.

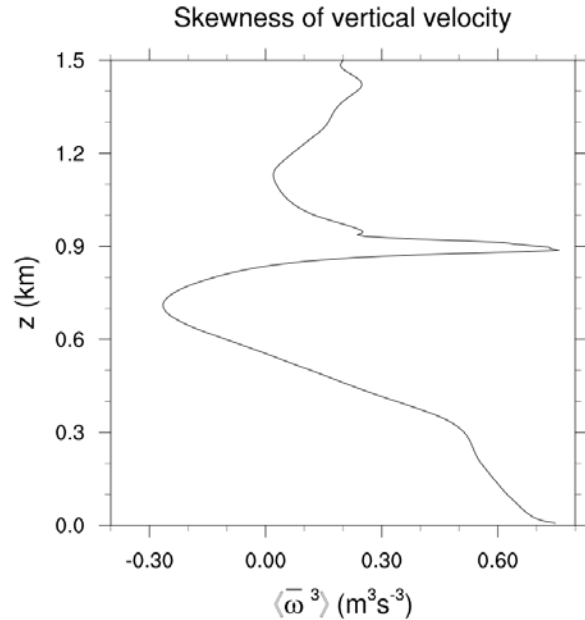


FIG. 7 Vertical profile of skewness of vertical velocity averaged over the last two hours of the simulation.

other hand, is associated with negative skewness where strong, narrow downdrafts are surrounded by larger areas of weaker updraft (Hogan et al., 2009 and Harvey et al., 2013).

The shape of the skewness profile matches the observations in the boundary layer, however, the simulated skewness has larger magnitudes than observations, at some altitudes by a factor of more than three (Fig. 7). At cloud base, our simulation matches observations by having a local minimum with negative skewness, providing evidence that cloud top radiative cooling drives turbulence within the cloud layer.

#### b. Comparison of coarse simulations using 5<sup>th</sup> order (default) and WENO advection scheme

Two coarse domains at 15 m vertical resolution were simulated using the 5<sup>th</sup> order scheme with mass flux correction (default method) and the WENO advection scheme, respectively. Henceforth, I refer to the simulation using the WENO scheme as the “WENO simulation,” and the simulation using the default advection scheme as the “base simulation.” The objective of this

study is to test how choice of advection scheme effects entrainment and the turbulent structure of the boundary layer, paying close attention to the solution at cloud top.

As depicted in Fig. 8, both base and WENO simulations produce significantly lower domain liquid water than the high resolution simulation and observations. Domain liquid water is the global integral of liquid water in the computational domain and is a measure of the thickness of the cloud layer. The WENO simulation rapidly diverges from the base within the first hour, reaching a domain liquid water content that is less than half that of the high resolution run at the end of the first hour.

The base coarse run also drops below the domain liquid water of the high resolution run in the first hour, however less drastically: ~10% reduction at the end of the first hour. As the simulations progress, both the base and WENO models generally decrease in domain liquid water, such that at the end of the fourth hour, the base model produces a domain liquid water content that is half of the high resolution model and the WENO model's domain liquid water content is even less-- a mere 8% of of the high resolution simulation. While the base model simulates a stabilizing/ growing domain liquid water after the 3<sup>rd</sup> hour, the WENO model shows no sign of stabilizing or increase in domain liquid water content.

both base and WENO, the cloud layer thins considerably in comparison to the high resolution simulation (Fig. 9). In the WENO simulation, the cloud layer almost entirely dissipates, retaining a marginal 0.06 g/ kg of liquid water mixing ratio at the end of the fourth hour. In contrast, the base model retains more liquid water, with a mixing ratio of ~0.20 g/kg at the end of the fourth hour, however still less than half the 0.45 g/kg observed.

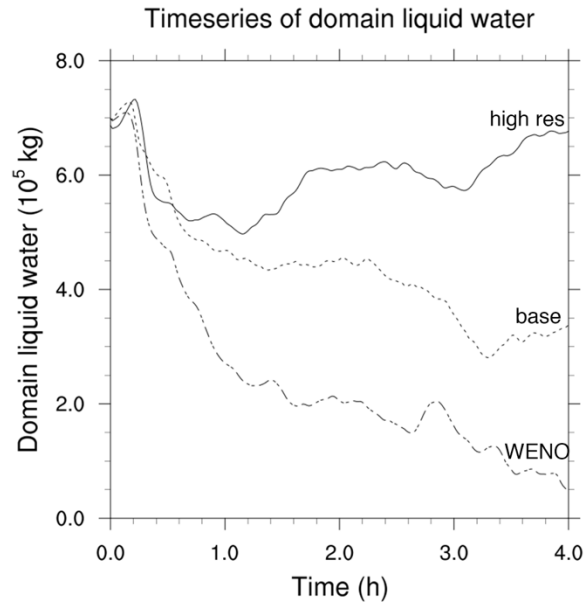


FIG. 8 Time series of domain liquid water for the high resolution simulation at 5 m (solid line), the base simulation at 15 m resolution (dotted line) WENO simulation at 15 m resolution (dashed line).

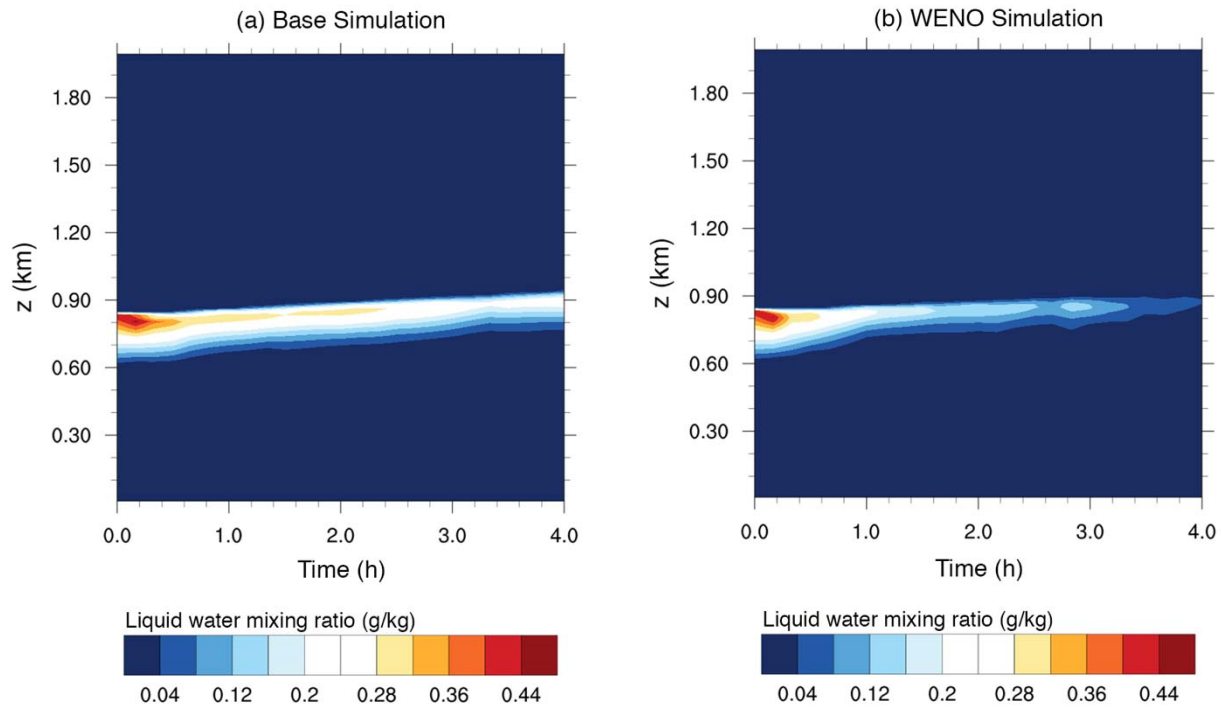


FIG. 9 Time series of the vertical profile of liquid water mixing ratio for the base (a) and WENO (b) simulations. The colors represent the liquid water mixing ratio  $q_t$ .

Both the base and WENO simulation exhibit a markedly different structure in variance of vertical velocity than the high resolution simulation. Although the high resolution simulation has a single peak in variance of vertical velocity, both coarse simulations exhibit bimodal structures with a local minimum near cloud-base, which is indicative of decoupling (Stevens 2000). Decoupling is when the cloud layer is separated from the sub-cloud layer, creating two separate layers with little to no exchange between the layers. The local minimum in variance occurring at cloud-base (600 m) suggests a zone of weak turbulent mixing, separating the sub-cloud layer (0 – 600m) from the cloud layer (600m – 1000m), forming a decoupled boundary layer (See appendix B for description of decoupling).

Overall, both coarse simulations produce significantly less variance of vertical velocity, and thereby turbulence, than the high resolution simulation and observations, with the WENO simulation producing the least turbulence of the three simulations.

The coarse and high resolution simulations have similarly shaped profiles of skewness of vertical velocity but with a different sign of skewness at cloud-base. At cloud base of 700 m, the high resolution run has negative skewness, indicating strong downdrafts while the coarse runs

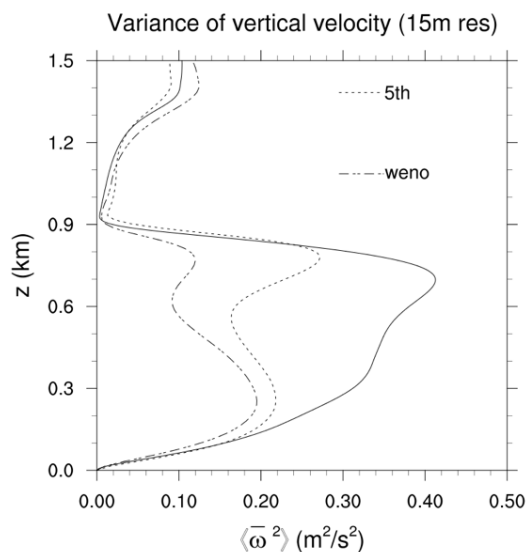


FIG. 10 Vertical profile of variance of vertical velocity averaged over the last two hours of the simulation for the high resolution (solid line) simulation, simulation using default advection scheme (dotted line) and the simulation using the WENO advection scheme (dashed line).

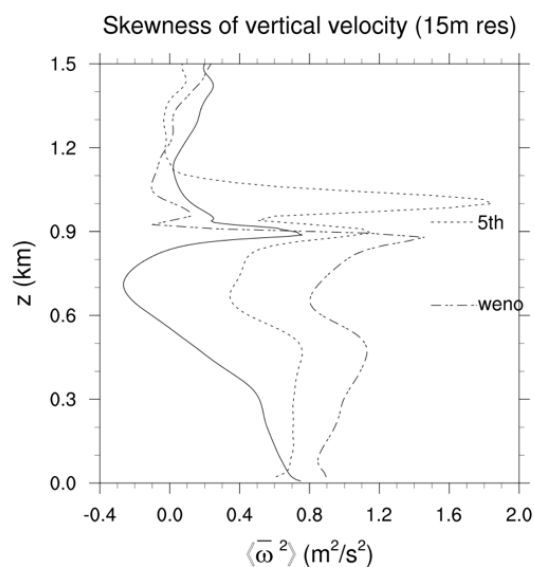


FIG. 11 Vertical profile of skewness of vertical velocity averaged over the last two hours of the simulation for the high resolution (solid line) simulation, simulation using default advection scheme (dotted line) and the simulation using the WENO advection scheme (dashed line).

also have a local minimum but the skewness is positive, indicating that surface/ cumulus convection dominates over radiative cooling. The positive skewness values throughout the entire profile indicate that surface/ cumulus convection is stronger than radiative cooling, suggesting an overall weakening of radiative cooling in both the base and WENO simulations as compared to the high resolution simulation. The two peaks present in the skewness profile for the base simulation may be artefacts of the two-hour averaging time window; resolving skewness peaks at different points in time.

In Fig. 12, it is evident that moisture tendency due to advection is more diffuse in WENO than in the high resolution simulation. In the high resolution simulation, moisture tendency due to advection is constrained to approximately 30 m around cloud top, whereas in base and WENO, large moisture tendencies due to advection are present in a wider vertical extent (40-50 m) around cloud top. This diffusion is likely a consequence of numerical diffusion caused by coarse resolution. Diffusion is stronger in the WENO simulation than the base simulation. Near high gradients, the WENO scheme adapts the stencil to a lower order stencil (3<sup>rd</sup> order) in an effort to produce a non-oscillatory solution. By using a lower order solution, however, the WENO scheme increases numerical diffusion. I believe this numerical diffusion leads to less

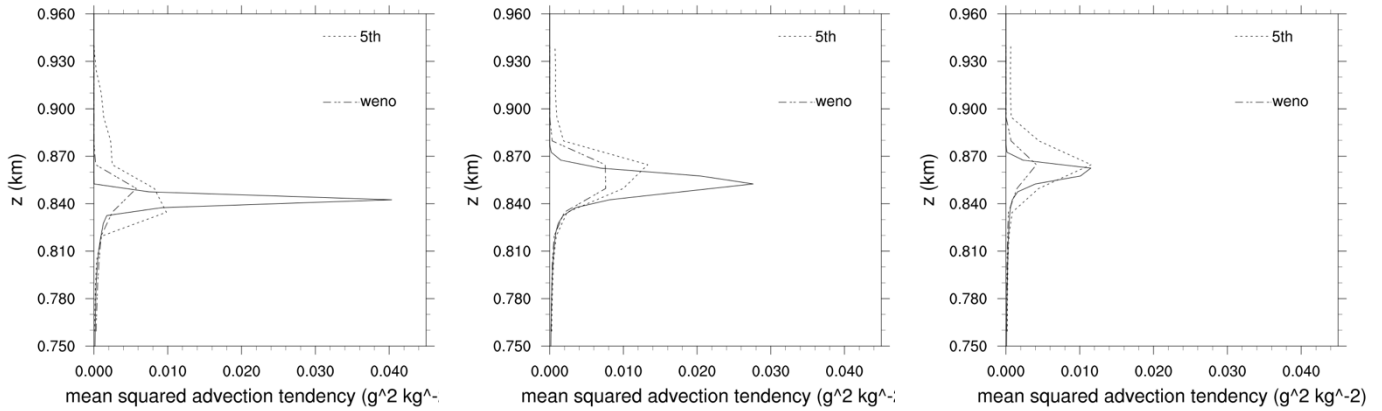


FIG. 12 Vertical profile of mean squared moisture tendency due to advection at (a) 20mins, (b) 40min and (c) 60 mins for the high resolution simulation (solid line), the base simulation (dotted line) and the WENO simulation (dashed line).

sharp gradients at the inversion and artificial entrainment of warm and dry air from the free Troposphere into the boundary layer.

Fig 13 further exemplifies the numerical diffusion, or “smoothing” of the scalar and vector fields, by the WENO scheme. In Fig. 13, total water perturbation  $q'_t$  is the total water mixing ratio deviation from the horizontal domain mean:  $q'_t = q_t - \bar{q}_t$ , and moisture tendency due to advection is the change in moisture with time caused by advection term:  $\left. \frac{dq}{dt} \right|_{adv}$ . While the high resolution and base simulation exhibit ample variability and high gradients in total water perturbation, the WENO simulation generates a smoother total water field with less variability and smaller gradients. This “smoothing” effect is isotropic, or the same in all directions, meaning that smoothing also occurs in the vertical, resulting in a less sharp inversion in temperature and moisture. This suggests increased flux across the inversion, leading to entrainment of dry air, resulting in a decrease in radiative cooling and consequently weaker eddies.

The snapshot of total water perturbation and wind vectors in Fig. 14 show a stable layer in the WENO simulation at  $z \approx 640\text{m}$  where upward velocities meet downward velocities, resulting in near zero velocities or a stable layer. Overall, the layer above  $640\text{m}$  appears to be driven by different processes than the layer below  $640\text{m}$  with different, sometimes opposing, wind directions and magnitudes. These characteristics signal a decoupled boundary layer, in alignment with earlier evidence of decoupling in the WENO simulation.

Fig 15 shows similar snapshots, overlaid with contours representing moisture tendency due to advection. In the 60 min snapshot, the high resolution run produces large advection tendency in a thin layer at cloud top, the base model also simulates large tendencies at cloud top but more spread-out in the vertical. The WENO simulation, on the other hand, shows small moisture tendency due to advection and drying (negative tendency represented by dashed lines) is evident.

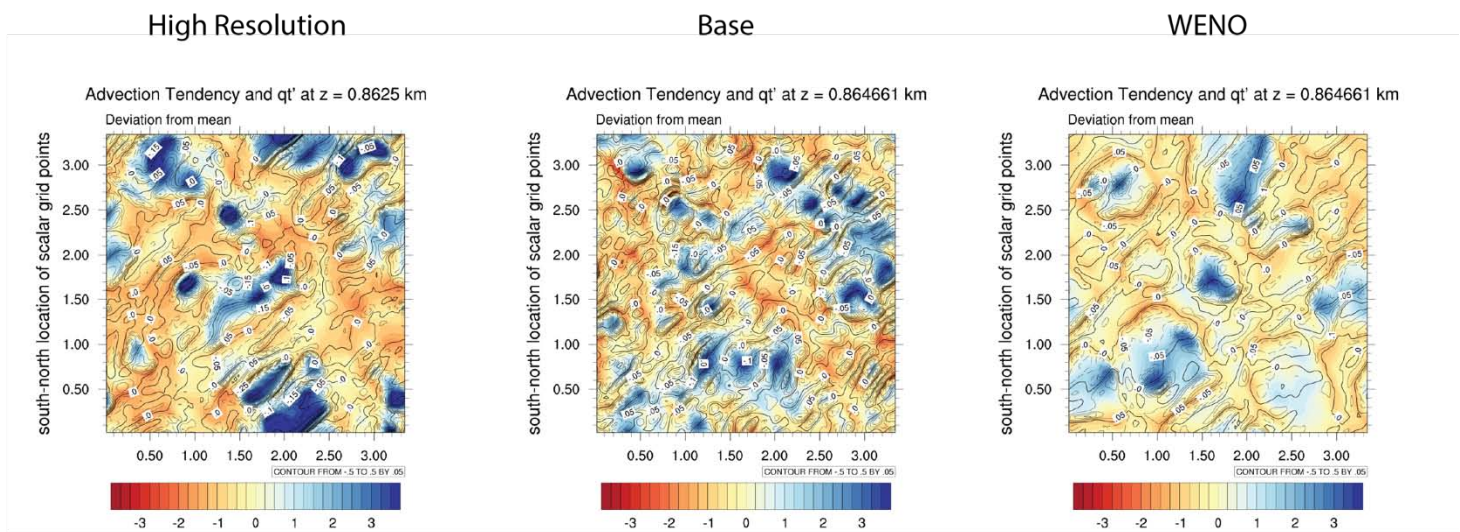


Fig. x. a horizontal cross-section at height  $z \approx 860\text{m}$ , the height of maximum advection tendency. This snapshot is taken 60 minutes into the simulation. The color map represents total water perturbation and the contours are advection tendencies for moisture. Results are shown for the high resolution simulation (a), base simulation (b) and WENO simulation (c).

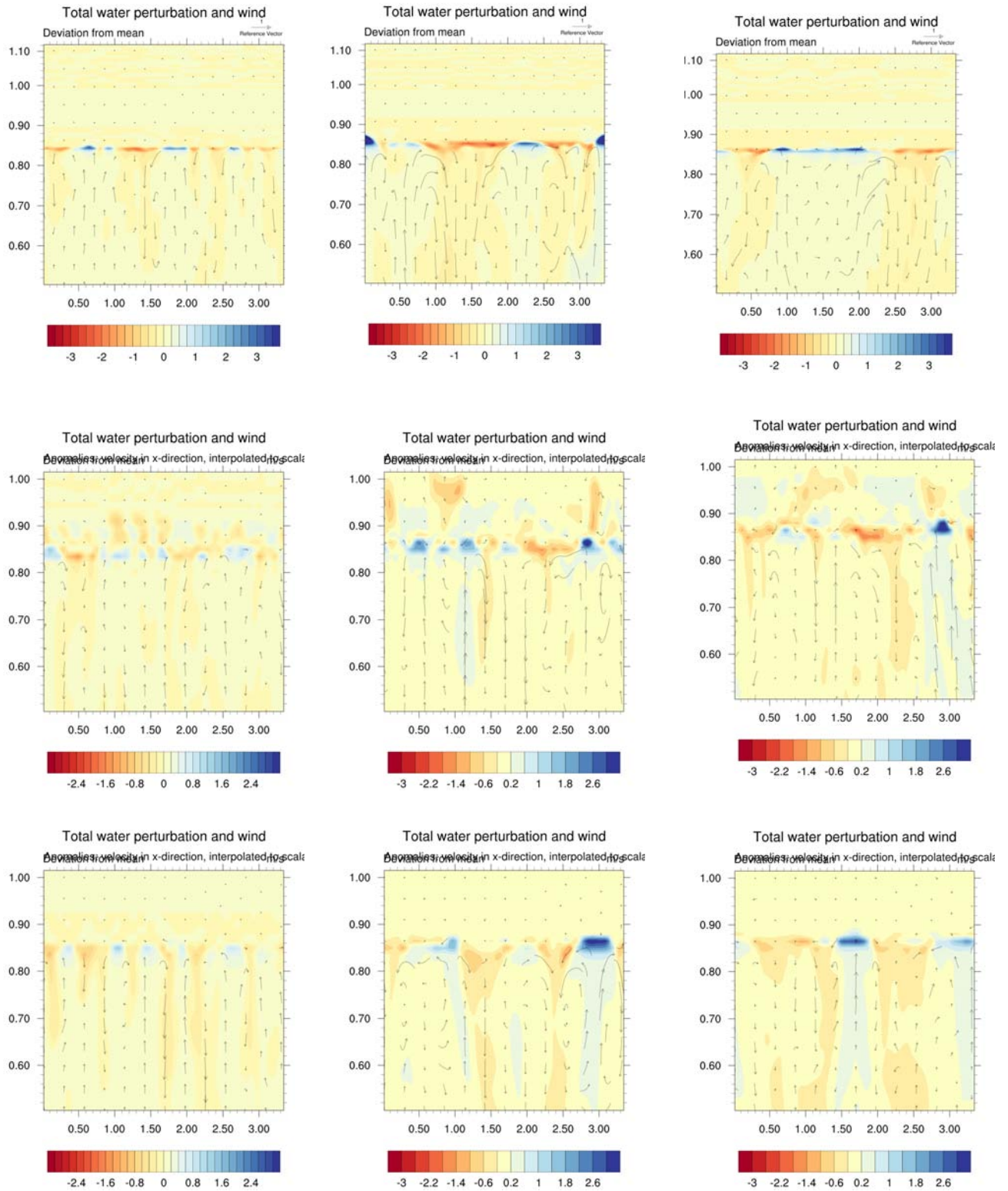
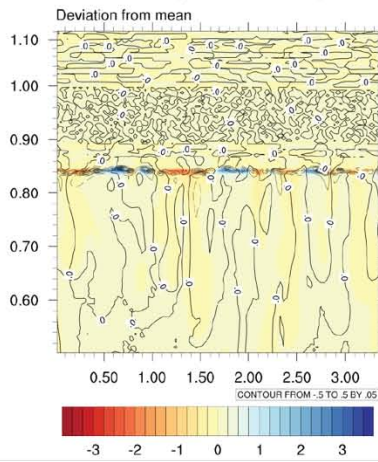


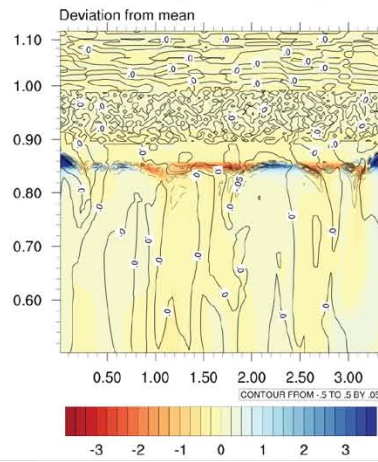
Fig. x, y, z. Horizontal, vertical (x, z) instantaneous snapshot of total water perturbation ( $q'_t = q_t - \bar{q}_t$ ) (color) and moisture tendency due to advection (contour) for the high resolution (top), base (middle) and WENO (bottom) simulations. The profiles are taken at  $y = 1.68\text{km}$  (middle of the domain) at (a) 20min, (b) 40min and (c) 60min

High Resolution

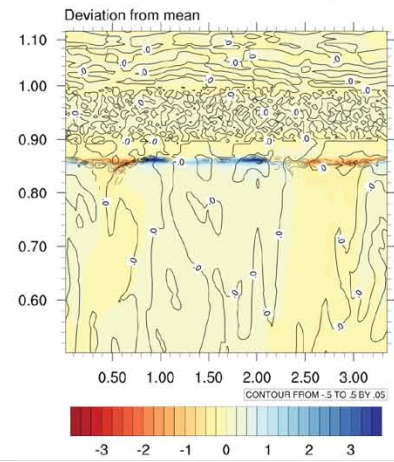
Advection Tendency and total water perturbation



Advection Tendency and total water perturbation

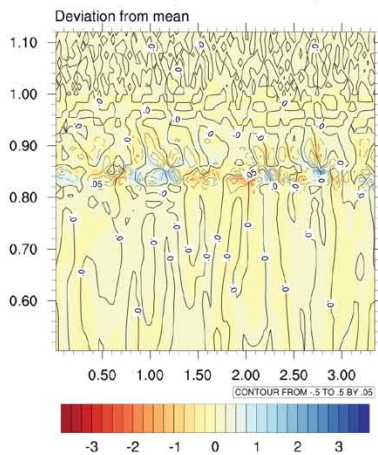


Advection Tendency and total water perturbation

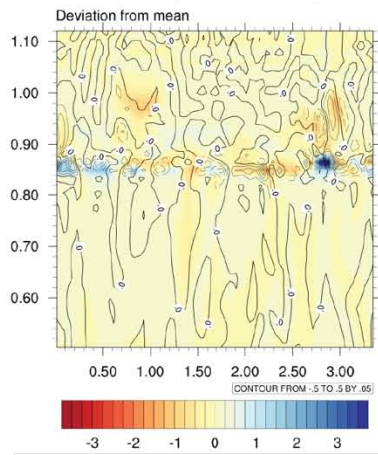


Base 15m resolution

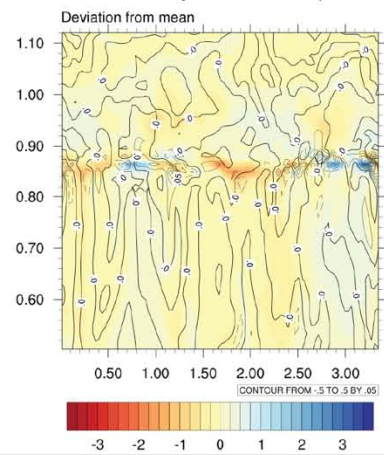
Advection Tendency and total water perturbation



Advection Tendency and total water perturbation

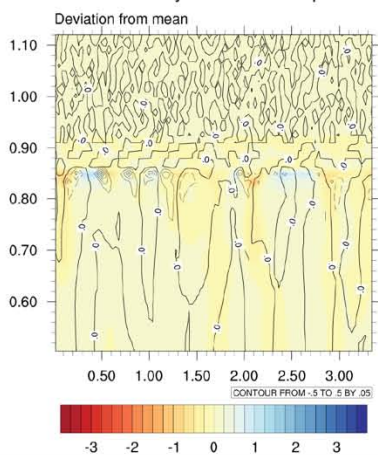


Advection Tendency and total water perturbation

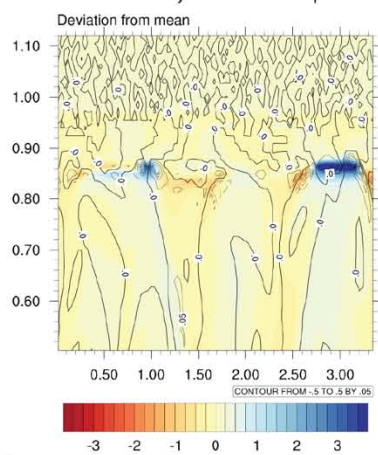


WENO 15m resolution

Advection Tendency and total water perturbation



Advection Tendency and total water perturbation



Advection Tendency and total water perturbation

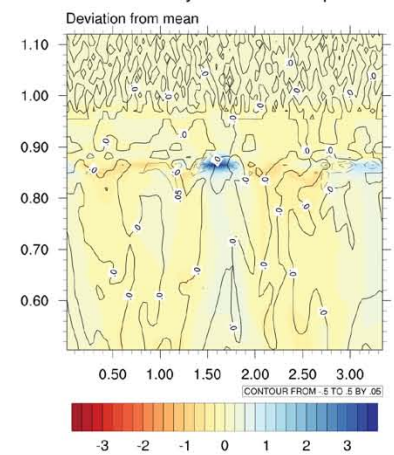


Fig. x,y,z. Vertical, horizontal (z, x) instantaneous profile of total water perturbation from the domain mean (color) and wind vectors for the high resolution (x), base coarse (y) and WENO coarse (z) simulation. The profiles are taken at y = 1.68km at 20min (a), 40min (b) and 60min (c).

## 5. Conclusion

The first research flight (RF01) of the DYCOMS II field campaign is a particularly fascinating test case because the cloud layer persisted throughout the night, despite conditions that many theories conjecture to result in decoupling or dissipation. While the WENO model simulated incorrect decoupling of the boundary layer and erroneous dissipation of the cloud, the default advection scheme produced a thinner, but still present, cloud layer that had closer agreement with the high resolution simulation and observations. The difference between the WENO and the default model results suggest that simulation of marine stratocumulus is highly sensitive to the numerics at cloud top. Near high gradients, the WENO algorithm adapts the stencil to a lower order stencil (between 3<sup>rd</sup> and 5<sup>th</sup> order) in an effort to reduce oscillations. Lower order solutions increase numerical diffusion. It is likely that this increased numerical diffusion led to artificial entrainment of dry air into the cloud layer and a resulting reduction in radiative cooling and turbulence. On the other hand, the base simulation used a 5<sup>th</sup> order scheme with mass flux correction producing a higher order (5<sup>th</sup> order) solution near the sharp inversion, although potentially with artificial oscillations in the solution. Results from our test case of marine stratocumulus suggests that a higher order (5<sup>th</sup> order) solution, not necessarily a non-oscillatory solution, led to more physically accurate simulation of the boundary layer.

The ideal advection scheme would be one that doesn't produce oscillations, has less numerical diffusion and retains the efficiency of schemes like WENO. Our results suggest that WENO is not the best choice for flow regimes that are highly dependent on small scale processes happening at a sharp inversion. However, if computational efficiency is a priority and transitions are less sharp, then WENO may be suitable. In the future, a higher order scheme that reduces numerical diffusion and oscillations at sharp gradients while retaining computational efficiency would improve simulation.

These results may inform modeling of other flow regimes with similar characteristics. For instance, cirrus clouds are often capped by a strong inversion at the tropopause and play a critical role in climate, since they have a net warming effect on the climate. Considering that clouds are the largest uncertainty in predictions of the Earth's changing energy balance, accurately modeling the behavior, scope, thickness and location of clouds is critical to narrowing the knowledge gap in climate and weather prediction.

## APPENDIX A

**Discretization of Navier Stokes equations**

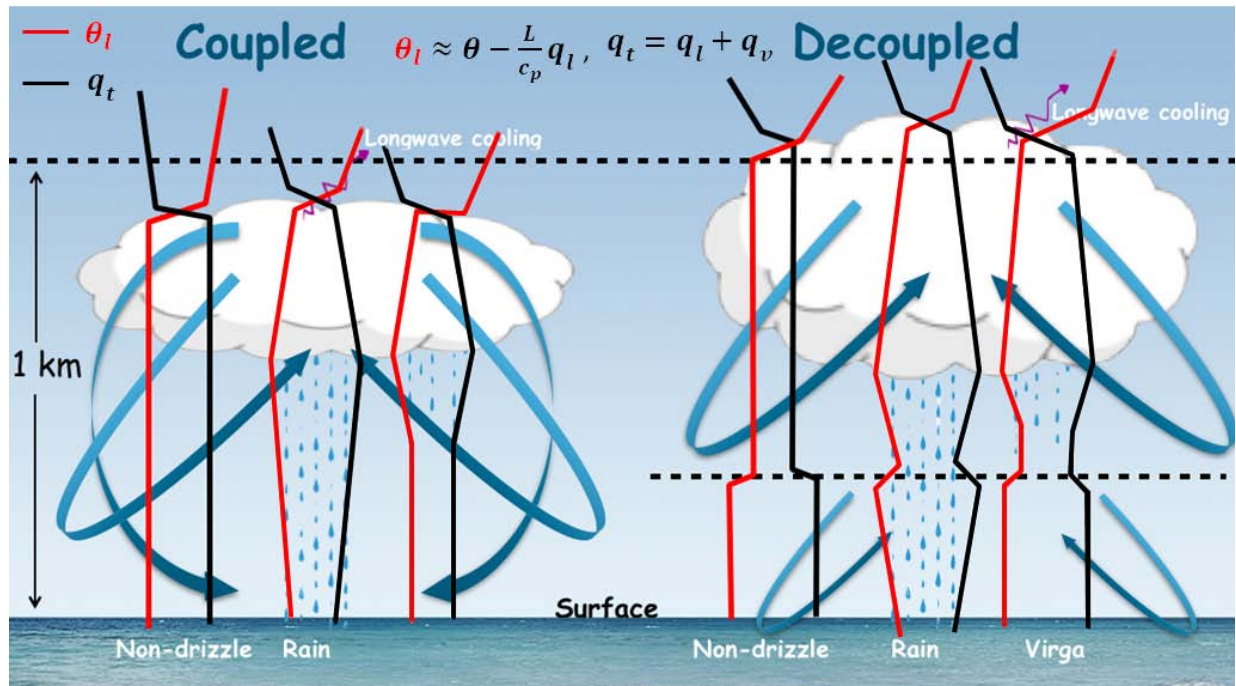
Because systems of nonlinear partial differential equations, like the compressible Navier Stokes equations, cannot be solved analytically, they must be approximated using numerical methods. There are several types of numerical schemes to solve partial differential equations, including spectral methods and finite difference methods. Most limited-area atmospheric models use finite difference methods. Finite difference methods approximate a continuous function with a set of discrete values, which inherently means some information is lost and the derivative can no longer be exactly solved. It is analogous to sampling in signal processing: some information about the signal is always lost since the sampling rate is finite. Instead, the derivative must be approximated from the values retained at each grid point. The difference between the approximated derivative and the exact solution is called the discretization, or truncation, error and it is inherent in finite difference schemes. The order of the finite difference scheme, meaning how many terms are included in the Taylor series approximation determines the size of error associated with that solution. Higher order solutions generate more accurate solutions since they retain more terms in the Taylor series expansion, yet the additional computational expense is often unjustified. As a result solutions higher than 4<sup>th</sup> or 5<sup>th</sup> order are not commonly used.

Because the Navier Stokes equations are a system of nonlinear partial differential equations, small errors can propagate with time and result in entirely different solutions after several time steps. For this reason, it is critical to minimize numerical errors in computation fluid dynamics.

## APPENDIX B

**Decoupled boundary layer**

In a coupled boundary layer, the air is well-mixed with potential temperature and total water mixing ratio relatively homogeneous through the PBL. In a decoupled boundary layer, the near-



surface layer is separated from the sub-cloud layer (not well-mixed) and the potential temperature and total water mixing ratio differ between layers. See figure below.

## REFERENCES

- Bretherton, C. S., M. K. Macvean, P. Bechtold, A. Chlond, W. R. Cotton, J. Cuxart, H. Cuijpers, M. Mhairoutdinov, B. Kosovic, D. Lewellen, C.-H. Moeng, P. Siebesma, B. Stevens, D. E. Stevens, I. Sykes and M. C. Wyant, 1999: An intercomparison of radiatively-driven entrainment and turbulence in a smoke cloud, as simulated by different numerical models. *Quart. J. Roy. Meteor. Soc.*, 125, 391–423
- Bryan, G. H., and J. M. Fritsch, 2002: A benchmark simulation for moist nonhydrostatic numerical models. *Mon. Wea. Rev.*, 130, 2917–2928.
- Deardorff, J. W., 1980a: Cloud top entrainment instability. *J. Atmos. Sci.*, 37, 131–147.
- Hogan, R. J., A. L. Grant, Illingworth, A. J., Pearson, G. N., and E. J. O’Connor, 2009: Vertical velocity variance and skewness in clear and cloud-topped boundary layers as revealed by Doppler lidar. *Q. J. Roy. Meteor. Soc.*, 135, 635–643.
- Harvey, N. J., R. J. Hogan, and H. F. Dacre, 2013: A method to diagnose boundary-layer type using Doppler lidar. *Q. J. Roy. Meteor. Soc.*, 139, 1681–1693.

- IPCC, 2013: Climate Change 2013: The Physical Science Basis. Contribution of Working Group I to the Fifth Assessment Report of the Intergovernmental Panel on Climate Change [Stocker, T.F., D. Qin, G.-K. Plattner, M. Tignor, S.K. Allen, J. Boschung, A. Nauels, Y. Xia, V. Bex and P.M. Midgley (eds.)]. Cambridge University Press, Cambridge, United Kingdom and New York, NY, USA.
- Jiang, G. and C.-W. Shu, 1996: Efficient implementation of weighted ENO schemes. *Journal of Computational Physics*, 126:202-228.
- Lewellen, D. C., and W. Lewellen, 1998: Large-eddy boundary layer entrainment. *J. Atmos. Sci.*, 55, 2645–2665.
- Lilly, D. K., 1968: Models of cloud topped mixed layers under a strong inversion. *Quart. J. Roy. Meteor. Soc.*, 94, 292–309.
- Randall, D. A., 1980: Conditional instability of the first kind upside-down. *J. Atmos. Sci.*, 37, 125–130.
- Shu, C.-W., 2003: High-order finite difference and finite volume WENO schemes and discontinuous Galerkin methods for CFD. *International Journal of Computational Fluid Dynamics*, 17:2, 107-118.
- Shu, C.-W., 2011: WENO methods. *Scholarpedia*, 6(5):9709.
- Stevens, B., C.-H. Moeng, and P. P. Sullivan, 1999: Large-eddy simulations of radiatively driven convection: Sensitivities to the representation of small scales. *J. Atmos. Sci.*, 56, 3963–3984.
- Stevens, B., 2000: Cloud transition and decoupling in shear-free stratocumulus-topped boundary layers. *Geophys. Res. Lett.*, 27, 2557–2560.
- Stevens, B., A. S. Ackerman, B. A. Albrecht, A. R. Brown, A. Chlond, J. Cuxart, P. G. Duynkerke, D. C. Lewellen, M. K. Macvean, R. Neggers, E. Sánchez, A. P. Siebesma, and D. E. Stevens 2001: Simulations of trade wind cumuli under a strong inversion. *J. Atmos. Sci.*, 58, 1870–1891.
- Stevens, B., 2002: Entrainment in stratocumulus mixed layers. *Quart. J. Roy. Meteor. Soc.*, 128, 2663–2690.
- Stevens, B., D.H. Lenschow, I. Faloona, C.-H. Moeng, D.K. Lilly, B.W. Blomquist, G. Vali, A.R. Bandy, T. Campos, H. Gerber, S. Haimov, B. Morely, and D.C. Thornton, 2003a: On entrainment in nocturnal marine stratocumulus. *Quart. J. Roy. Meteor. Soc.*, 129, 3469–3492.
- Stevens, B., D. H. Lenschow, G. Vali, H. Gerber, A. Bandy, B. Blomquist, J-L. Brenguier, C. S. Bretherton, F. Burnet, T. Campos, S. Chai, I. Faloona, D. Friesen, S. Haimov, K.

- Laursen, D. K. Lilly, S. M. Loehrer, Szymon P. Malinowski, B. Morley, M. D. Petters, D. C. Rogers, L. Russell, V. Savic-Jovicic, J. R. Snider, D. Straub, Marcin J. Szumowski, H. Takagi, D. C. Thornton, M. Tschudi, C. Twohy, M. Wetzel, and M. C. van Zanten, 2003b: Dynamics and Chemistry of Marine Stratocumulus -- DYCOMS-II. *Bull. Amer. Meteor. Soc.*, 84, 579–593.
- Stevens, B, CH Moeng, and AS Ackerman, 2005: Evaluation of large-eddy simulations via observations of nocturnal marine stratocumulus. *Monthly weather* 133: 1443 – 1462.
- Moeng, C.-H., W. R. Cotton, C. Bretherton, A. Chlond, M. Khairoutdinov, S. Krueger, W.S. Lewellen, M. K. MacVean, J. R. M. Pasquier, H. A. Rand, A. P. Siebesma, B. Stevens, and R. I. Sykes, 1996: Simulation of a stratocumulus-topped PBL: Intercomparison among different numerical codes. *Bull. Amer. Meteor. Soc.*, 77, 261–278.
- Stevens, B., A. Beljaars, S. Bordoni, C. Holloway, M. Köhler, S. Krueger, V. Savic-Jovicic, and Y. Zhang, 2007: On the Structure of the Lower Troposphere in the Summertime Stratocumulus Regime of the Northeast Pacific. *Mon Weather Rev*, 135, 985–1005.
- Warren, S. G., C. J. Hahn, J. London, R. M. Chervin, and R. L. Jenne, 1986: Global distribution of total cloud cover and cloud types over land. NCAR Tech. Note NCAR/TN-2731STR, National Center for Atmospheric Research, Boulder, CO, 29 pp. 1 200 maps.
- Warren, S. G., C. J. Hahn, J. London, R. M. Chervin, and R. L. Jenne, 1988: Global distribution of total cloud cover and cloud types over ocean. NCAR Tech. Note NCAR/TN-3171STR, National Center for Atmospheric Research, Boulder, CO, 42 pp. 1 170 maps.
- Wilhelmson, R. B., and C.-S. Chen, 1982: A simulation of the development of successive cells along a cold outflow boundary. *J. Atmos. Sci.*, 39, 1466-1483.